Neuron
Article

Theta Oscillations Provide Temporal Windows for Local Circuit Computation in the Entorhinal-Hippocampal Loop

Kenji Mizuseki,[1] Anton Sirota,[1] Eva Pastalkova,[1] and György Buzsáki[1,*]
[1]Center for Molecular and Behavioral Neuroscience, Rutgers, The State University of New Jersey, 197 University Avenue, Newark, NJ 07102, USA
*Correspondence: buzsaki@axon.rutgers.edu
DOI 10.1016/j.neuron.2009.08.037

SUMMARY

Theta oscillations are believed to play an important role in the coordination of neuronal firing in the entorhinal (EC)-hippocampal system but the underlying mechanisms are not known. We simultaneously recorded from neurons in multiple regions of the EC-hippocampal loop and examined their temporal relationships. Theta-coordinated synchronous spiking of EC neuronal populations predicted the timing of current sinks in target layers in the hippocampus. However, the temporal delays between population activities in successive anatomical stages were longer (typically by a half theta cycle) than expected from axon conduction velocities and passive synaptic integration of feed-forward excitatory inputs. We hypothesize that the temporal windows set by the theta cycles allow for local circuit interactions and thus a considerable degree of computational independence in subdivisions of the EC-hippocampal loop.

INTRODUCTION

When neuronal signals propagate through multiple anatomical regions, representation of the initiating event is not merely transferred from one layer to the next but changes progressively, largely determined by the state and computational properties of successive layers. Local computation requires time, and the temporal windows of such computations are often determined by oscillations, reflected by local field potentials (LFP; cf., Buzsáki, 2006). Due to the laminar anatomy of the hippocampus and entorhinal cortex (EC), LFP patterns observed in these structures reflect various behavior-dependent network dynamics. The theta rhythm (5–10 Hz in the rat) is the most prominent LFP pattern in the hippocampal-entorhinal system (Grastyán et al., 1959; Holmes and Adey, 1960; Vanderwolf, 1969; Mitchell and Ranck, 1980; Alonso and García-Austt, 1987). Theta frequency pacing of network excitability can provide temporal packaging and transfer of neuronal information (Skaggs et al., 1996; Hasselmo et al., 2002; Hasselmo, 2005; Dragoi and Buzsáki, 2006; Sirota et al., 2008) and is thought to be critical for synaptic plasticity (Pavlides et al., 1988; Huerta and Lisman, 1995). Theta oscillations are suggested to coordinate the encoding and retrieval of episodic and spatial memories (Hasselmo, 2005; O'Keefe and Burgess, 2005; Jensen and Lisman, 2005) and interfering with the rhythm results in behavioral deficits, reminiscent of partial hippocampal damage (Winson, 1978). However, the physiological mechanisms that give rise to theta LFP, the temporal coordination of individual neurons across anatomically successive subregions by theta oscillations (Bland 1986; Buzsáki, 2002) and especially the role of theta-coordinated time frames for securing relative independence for computations in different subdivisions in the EC-hippocampal system are not well understood.

According to the simplest model of theta generation, the medial septum/diagonal band of Broca in the basal forebrain functions as a pacemaker enforcing a global rhythm into which hippocampal and EC networks are entrained (Petsche et al., 1962; Stewart and Fox, 1990). However, numerous studies, including pharmacological interventions (Vanderwolf, 1988), deafferentation (Buzsáki et al., 1983; Bragin et al., 1995), inactivation (Mizumori et al., 1990), intracellular/intradendritic recordings (Fox 1989; Soltesz and Deschénes, 1993; Kamondi et al., 1998), multisite recording (Kocsis et al., 1999; Montgomery et al., 2008), current-source density (CSD) measurements (Buzsáki et al., 1986; Brankack et al., 1993; Bragin et al., 1995; Montgomery et al., 2009), in vitro studies (Konopacki et al., 1987; Traub et al., 2004), and computational modeling (Leung, 1984; Traub et al., 2004; Rotstein et al. 2005; Orban et al., 2006), indicate that multiple rhythm generators and theta dipoles (i.e., paired sinks and sources of extracellular currents) are at work in both the hippocampus (Buzsáki, 2002; Montgomery et al., 2009) and the EC (Mitchell and Ranck, 1980).

The importance of entorhinal inputs in theta generation has been highlighted by previous works (Mitchell and Ranck, 1980; Buzsáki et al., 1983; Alonso and García-Austt, 1987; Stewart et al., 1992; Chrobak and Buzsáki, 1998). The main excitatory input to the dentate gyrus and CA3 region derives from EC layer II (EC2) stellate cells (Steward, 1976), whereas the EC projections to CA1 originate mainly in layer III (Steward and Scoville, 1976; Amaral and Witter, 1989). In accordance with the laminar arrangement of EC projections (Amaral and Lavenex, 2007), theta current sinks are present in the CA1 stratum lacunosum-moleculare and the midmolecular layer of the dentate gyrus. Because the sinks in these respective layers are 180° out of phase (Buzsáki et al., 1983, 1986; Brankack et al., 1993; Kamondi et al., 1998;

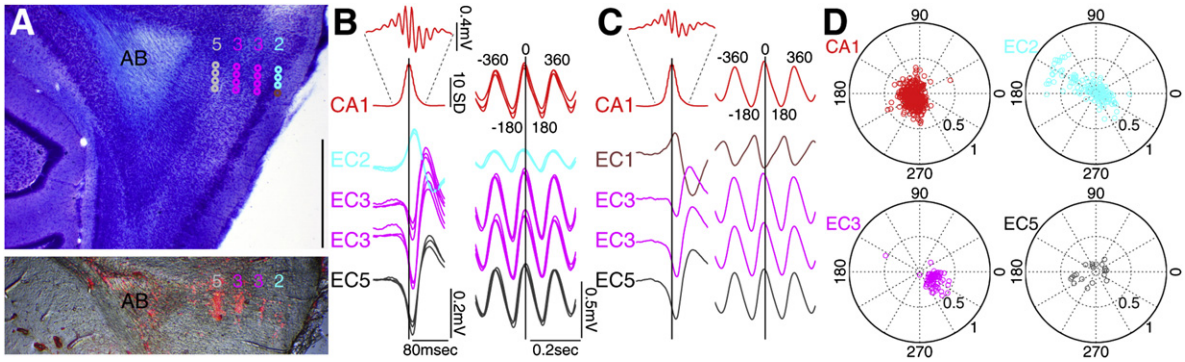

Figure 1. Physiological Identification of EC Cell Layers

(A) Top: Nissl-stained EC sagittal section with reconstructed tracks of the four-shank silicon probe (200 μm intershank distance). Bottom: the same section with DiI fluorescence labeling. Recording locations in each session were estimated from the magnitude of probe movement by the experimenter and from physiological parameters, shown in (B) and (C). Brown, EC1; light blue, EC2; magenta, EC3; gray, EC5 recording sites. Scale bar = 1 mm. AB, angular bundle.

(B) Left two top traces (red), mean ripple power from the CA1 pyramidal cell layer (normalized by standard deviation) and averaged ripple trace at a higher temporal resolution. Left bottom four traces, CA1 ripple power-centered average traces (n = 1656–2590) of EC sharp waves across different layers. Traces from three different sessions in progressively deeper sites (corresponding to circles in A) are superimposed. Note the polarity reversal of EC sharp waves between EC2 and lower layers. Right, averaged theta waves, centered on the peak of the CA1 pyramidal layer theta from the same sessions.

(C) As in (B) but with the tip of the rightmost shank in EC1 (last recording session). Note the phase-reversed theta signals between EC1 and lower layers.

(D) Polar plots of principal neurons in CA1 and different layers of EC (EC2, EC3, and EC5) referenced to theta oscillation in CA1 pyramidal layer. Each circle represents preferred phase (peak of theta = 0, 360°, trough = 180° in all figures) and modulation depth (mean resultant length or $\overline{R}$, 0–1, represented by the distance from the center of the plot) of a single neuron. All data (A–D) are from the same rat (ec14). Layer and region-specific color coding apply to all figures. Positive polarity is up in all figures.

Kocsis et al., 1999), it has been hypothesized that they may reflect anti-phase firing of EC3 and EC2 principal neurons, respectively (Montgomery et al., 2009). An unsolved paradox, however, is that CA1 pyramidal neurons fire with the lowest probability at times of the maximum inward current (sink) in the distal apical dendrites located in stratum lacunosum-moleculare (Kamondi et al., 1998; Csicsvari et al., 1999; Buzsáki, 2002). Why are there such long delays between dendritic depolarization, reflected by the theta sink, and the preferred discharge phase of CA1 pyramidal cells? Furthermore, CA3 and CA1 pyramidal cells preferentially fire at different phases of the theta cycle (Dragoi and Buzsáki, 2006), raising questions about the mechanisms responsible for controlling the firing of the CA1 principal neurons (Brun et al., 2002; Hasselmo et al., 2002; Hasselmo, 2005). An important further "complication" is that active neurons in the hippocampus and EC do not have a fixed theta phase preference; their phase varies systematically as a function of behavior (O'Keefe and Recce, 1993; Hafting et al., 2008), pointing to a role of the local circuits in controlling place cell discharges (Tsodyks et al., 1996; Hasselmo et al., 2002).

To understand the mechanisms that regulate temporal coordination of neuronal activities in the EC-hippocampus system, we simultaneously recorded LFP and multiple single neuronal activities in the different layers of these structures in various behavioral tasks and examined the temporal relationships of neuronal activity between different subregions. We found that principal cells in several monosynaptically connected layers/regions fired with significantly longer theta phase offsets and temporal delays than would be expected by axonal conduction times, synaptic delays, and passive synaptic integration. We hypothesize that the temporal windows set by the theta cycles allow for local circuit interactions. As a result, population activity in a downstream layer does not merely reflect an upstream "drive" but also represents the result of autonomous local computation.

RESULTS

LFP and unit firing were recorded simultaneously in multiple layers of the dorsocaudal medial EC and either the CA1 or CA3 pyramidal layer or the granule cell layer of the dentate gyrus (DG) of dorsal hippocampus in five rats (see Table S1 available online). Recordings were carried out while the animal explored an open field (180 cm by 180 cm or 120 cm by 120 cm), ran on a linear track (250 cm long) or performed in a T maze alternation task or a rewarded wheel-running task (Pastalkova et al., 2008).

Physiological Identification of Entorhinal Cortical Layers

The four-shank silicon probe was gradually advanced between recording sessions, and the position of the recording sites in individual sessions was determined from the combination of physiological data and histological verification of the electrode tracks (Figures 1A–1C and S1). The lamina dissecans (layer IV) of Nissl-stained sections allowed for a distinction between superficial and deep layer neurons of the EC. The distinct physiological LFP patterns in different layers (Chrobak and Buzsáki, 1996, 1998) provided further precision for on-line verification of the recorded layers. Sharp-wave ripples recorded from the CA1 pyramidal layer were associated with a negative wave in EC3 to EC6, with a polarity reversal between EC2 and EC3 layers (Figure 1B; Chrobak and Buzsáki, 1996; see also Figure S2). In contrast, theta waves were in phase from EC3 to EC6 and reversed between EC1 and EC3 (Figure 1C; Mitchell and Ranck, 1980; Alonso and García-Austt, 1987; Chrobak and Buzsáki, 1998;

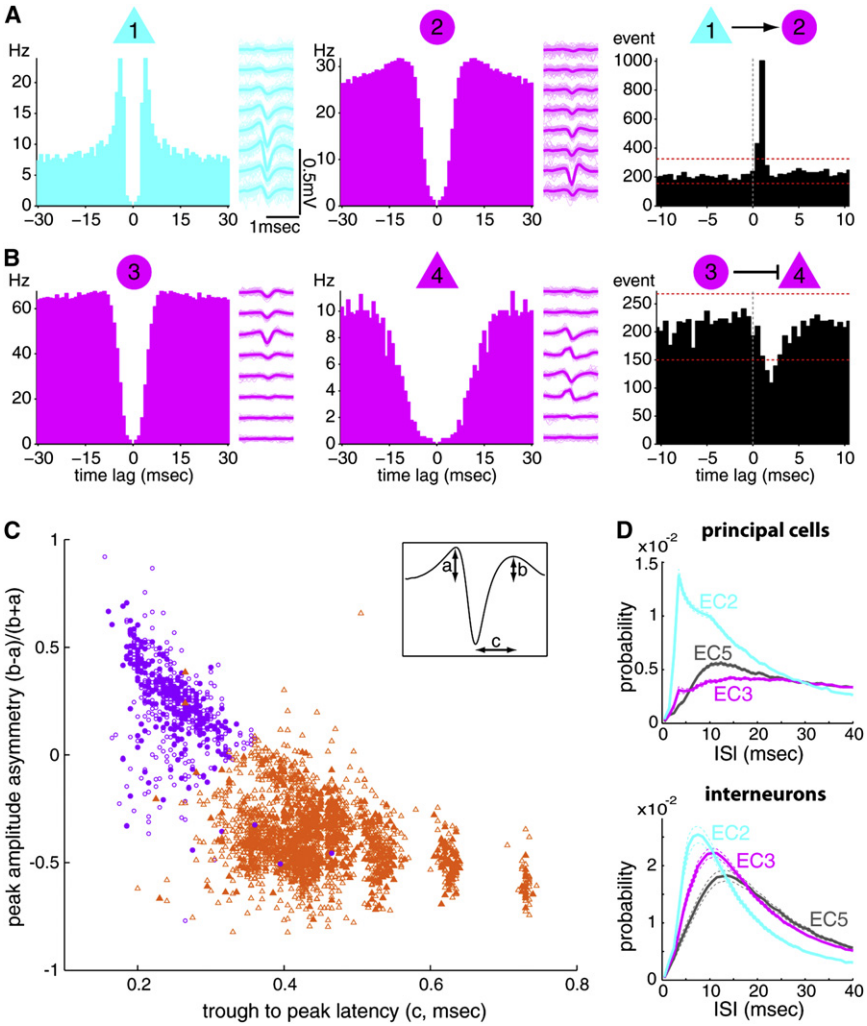

Figure 2. Separation of Putative Entorhinal Principal Cells and Interneurons

(A) Autocorrelograms and average filtered (0.8–5 kHz) waveforms of a putative EC2 principal cell (light blue) and an EC3 interneuron (magenta). Right: cross-correlogram revealed short-latency monosynaptic interactions between the neuron pair. Neuron 1 excites neuron 2 (these neurons were recorded from two different electrodes). Dashed lines indicate 1% and 99% global confidence intervals estimated by spike jittering on a uniform interval of [−5,5] ms (Fujisawa et al., 2008).

(B) Same display as in (A) but for an EC3 interneuron-principal cell pair (also recorded from two different electrodes). Note short-latency suppression of spikes in the target neuron.

(C) Putative principal cells and interneurons (empty symbols; orange, 1490 principal cells, violet, 327 interneurons) separated by waveform asymmetry and trough-to-peak latency (see inset; 0.8–5 kHz; Sirota et al., 2008) and other criteria (see Supplemental Experimental Procedures). Filled orange and violet symbols correspond to excitatory (557 cells) and inhibitory (263 cells) neurons, respectively identified by monosynaptic interactions (as in A and B; see also Figure S3). Total of 2744 EC neurons.

(D) Interspike intervals (mean ± SEM) of EC principal cells and interneurons. Bin size = 1 ms.

Hafting et al., 2008). Since we could not always reliably distinguish between EC5 and EC6, for simplicity we refer to all deep layer neurons as EC5. Neurons at transition zones whose layer membership could not be identified were excluded from the analyses (Figure S1, yellow circle). To facilitate the comparison of timing relationships between different subregions, the theta oscillations derived from EC3 LFP was used as a common reference to examine spike-theta phase relationship in different regions and layers, unless mentioned otherwise (Figures 1D, S10, and S14). EC3 theta was typically in phase (<90° shift in all experiments) and highly coherent (0.6–0.9; Chrobak and Buzsáki, 1998) with theta recorded from the CA1 pyramidal layer of the dorsal hippocampus (Figures 1B and 1C).

Physiological Identification of Entorhinal Neuron Types

Since the various classes of principal cells and inhibitory interneurons have different circuit and resonant properties and contribute differentially to cortical operations (Freund and Buzsáki, 1996; Markram et al., 2004; Somogyi and Klausberger, 2005), experimental classification of principal cells and inhibitory interneurons is important for studying their contribution to coordinated oscillatory activity. Whereas a consensus exists on the physiological features distinguishing pyramidal cells and interneurons in the CA1–CA3 regions of the hippocampus (Buzsáki et al., 1983; Csicsvari et al., 1999), there are no generally accepted methods for the segregation of EC principal cells and interneurons (Frank et al., 2001; Hafting et al., 2005; 2008; Isomura et al., 2006). We took advantage of the simultaneously recorded EC cells to physiologically identify units as excitatory or inhibitory neurons by their short-latency temporal interactions with other neurons (Barthó et al., 2004; Sirota et al., 2008). Putative monosynaptic connections are associated with precisely timed spiking relationships at short (<5 ms) latency offsets between two recorded neurons, as detected by narrow significant peaks or troughs in the cross-correlogram (Figures 2A, 2B, and S3; Supplemental Data; Csicsvari et al., 1998; Frank et al., 2001; Constantinidis et al.,2002; Barthó et al., 2004; Maurer et al., 2006b; Fujisawa et al., 2008). Approximately 30% of EC neurons were identified physiologically by their monosynaptic interactions (820 out of 2744 neurons in five rats). These physiologically identified excitatory and inhibitory neurons (Figures 2C and S3A, filled symbols), in turn, served as a template for exploring other spike features, which could best segregate principal cells and interneurons, such as waveform asymmetry and trough-to-peak latency (Figure 2C, empty symbols; Sirota et al., 2008). By these criteria, the majority of the EC neurons were classified as putative principal cells (2047 neurons, 74.6%; Figure 2C,

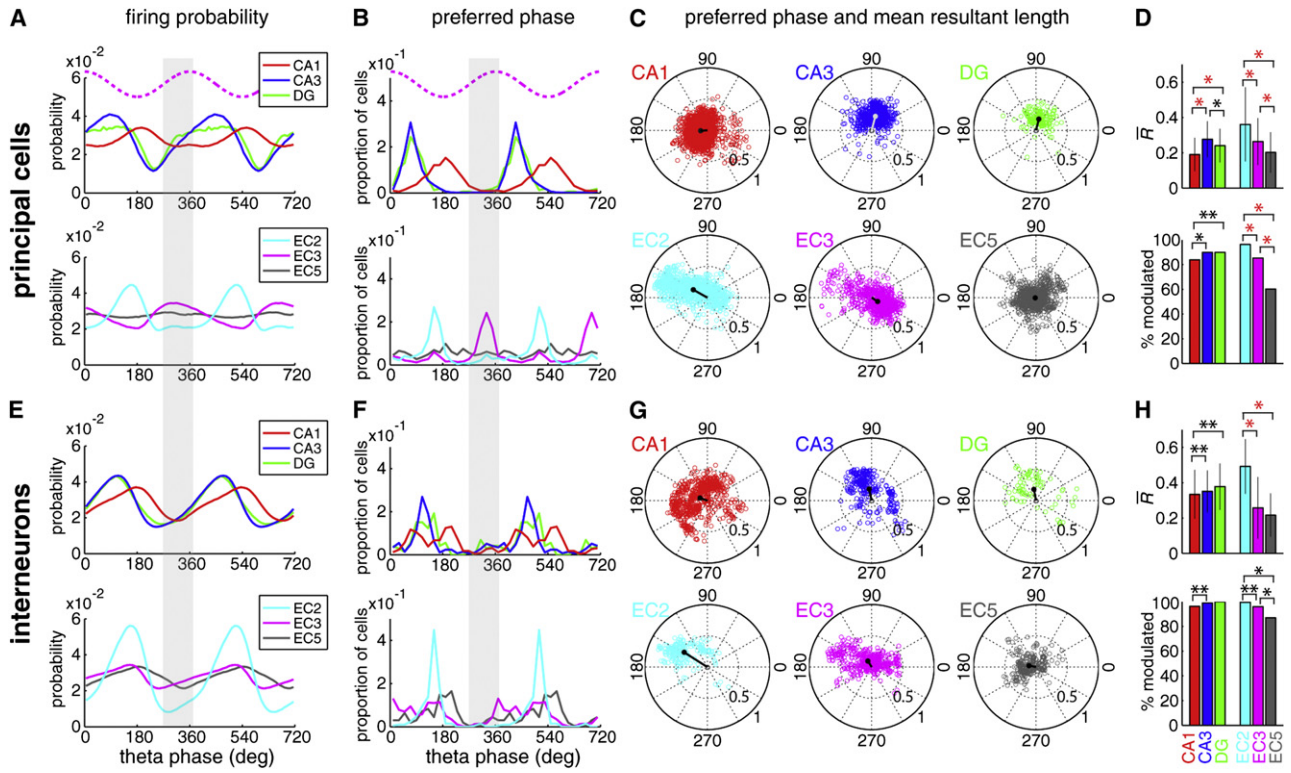

Figure 3. Theta Phase Modulation of Hippocampal and EC Neurons

(A) Population discharge probability of principal neurons from different subregions as a function of EC3 theta phase (top dotted magenta traces in A and B, idealized reference theta cycle in EC3). Spikes from all principal neurons were included, independent of whether or not the neuron was significantly modulated by theta phase. Two theta cycles are shown to facilitate visual comparison. DG, dentate gyrus cells. Bin size = 10°. Note the deviation of most histograms from an idealized sinusoidal pattern.

(B) Distribution of preferred phase of single neurons. Note that the majority of EC3 neurons occupy a phase space (ascending phase of EC3 theta), in which the discharge probability of all other neurons groups is at minimum (shaded columns in A, B, E, and F). Bin size = 20°.

(C) Polar plots of preferred phase and modulation depth (mean resultant length) of single neurons (circles) and group mean (lines). Only neurons with significant theta modulation (with at least 50 spikes and firing rate >0.1 Hz; Rayleigh test, $p < 0.01$) are included in (B) and (C). Note the largest mean resultant length in EC2 and in a small subset of EC3 principal cells with a phase preference opposite to the majority of the EC3 population.

(D) Magnitude of modulation depth by the theta cycle (mean $\overline{R}$ ± standard deviation; only significantly theta-modulated neurons are included) and the percentage of neurons significantly modulated by the theta cycle. **$p < 0.05$, *$p < 10^{-4}$, red *$p < 10^{-11}$, Wilcoxon rank sum test (mean resultant length) and chi-square independence test (proportion of significantly modulated cells).

(E–H) Same display for interneurons.

orange triangles), and the minority as putative interneurons (590 neurons, 21.5%; Figure 2C, purple circles; Table S1). EC2 principal neurons, as a group, could be distinguished from EC3 and EC5 principal neurons by their higher propensity to burst at short interspike intervals (<6 or 10 ms; Figures 2D and S4). Though consistent with previous neuron identification in the neocortex (Sirota et al., 2008), our tentative neuron type classification requires independent verification, using more direct methods, in future experiments.

Theta-Phase Relationship of Entorhinal and Hippocampal Neurons

Although both the amplitude and frequency of theta LFP show regional variations with behavior (cf. Buzsáki 2002), theta signals, on average, were highly coherent between the hippocampus and EC (Figures 1B and 1C). To examine the spike-theta phase relationship of neurons, we used two complementary measures: theta phase distribution of all the spikes in the population (Figures 3A and 3E) and the distribution of preferred phases of single neurons (Figures 3B and 3F). Principal cells and interneurons had unique and region-specific theta phase preferences (Figure 3). A striking observation was the synchrony and similar phase preference of the interneurons in all regions. Although interneuron groups in different regions could have a single peak, double peaks or broad distributions of preferred phases (Figure 3F), the overall probability of discharge was at a minimum on the ascending phase of the reference theta waves (shaded columns in Figures 3A, 3B, 3E, and 3F; Figure S5) recorded in EC3 (approximately in phase with theta derived from the CA1 pyramidal layer; Figure 1). Dentate putative principal neurons and CA3 pyramidal cells shared a similar phase space, preceding the firing of CA1 pyramidal cells by 90°–120° (Buzsáki et al., 1983; Skaggs et al., 1996; Dragoi and Buzsáki 2006). EC2 and EC3 principal neurons, the main afferents to dentate/CA3

and CA1 neurons, respectively (Steward, 1976; Steward and Scoville, 1976; cf. Amaral and Witter, 1989), fired, on average, out-of-phase from each other and, unexpectedly, had preferred discharge phases approximately *opposite* to those of their target hippocampal neurons. A small subset of EC3 pyramidal cells though fired in phase with the EC2 population (Figures 3B and 3C), and this subgroup showed the strongest theta phase locking (i.e., largest mean resultant lengths) of all EC3 cells (Figure 3C). Although a subset of individual EC5 principal neurons had significant theta phase locking, their preferred phases showed a relatively uniform distribution in the population (Figures 3B–3D). As a result, the EC5 principal cells were least modulated by the theta cycle as a population (Figure 3A; Chrobak and Buzsáki, 1994, 1998; Frank et al., 2001). Overall, with the exception of EC3 pyramidal cells, principal cells and interneurons in the hippocampus and EC were least active on the ascending phase of the EC3 theta (shaded phase range in Figures 3A, 3B, 3E, and 3F; Figure S5). In the EC, EC2 neurons showed the strongest theta modulation as a population (Figures 3A, 3E, and S4) and had the highest percentage of theta-modulated cells (Figures 3D and 3H). The validity of the phase distribution described above was confirmed when only physiologically identified principal cells and interneurons were considered (Figure S6) and when neuron groups from individual rats were examined separately (Figure S7).

In addition to the overall results (Figure 3) collected from all behavioral tests, we also analyzed the unit-LFP relationships separately from sessions recorded during exploration in the open field, running on a linear track and performance in the T maze and rewarded wheel-running task. Although slight variations were observed, the theta phase relations of neurons in different EC layers and hippocampal regions were essentially identical across different testing conditions (Figure S8). We also tested whether using different methods for the calculation of theta phase would affect the overall statistics (Siapas et al., 2005). Similar results were obtained using the peak or trough (Csicsvari et al., 1999) or the Hilbert transform of the theta band-filtered LFP to compute theta phase (Figure S9). Finally, in sessions where CA1 and EC recordings were made simultaneously, we used either the CA1 pyramidal layer or the EC3 LFP and obtained identical relative phase distributions (Figure S10). In summary, the theta phase-relationships of neuron populations in different EC-hippocampal layers/regions showed much longer theta phase (time) offsets than could be explained by the passive integration of excitatory inputs by the target neurons.

Temporal Relationship between Entorhinal and Hippocampal Neurons

To examine more directly the spike timing relationships among neuronal groups in the EC-hippocampal system, we also computed group cross-correlograms between cell pairs of all layers/regions and the temporal offsets of individual pairs (Figure 4, gray and black histograms, respectively. See Supplemental Experimental Procedures and Figure S11 for cross-correlograms of individual neuron pairs). In support of the theta LFP-unit analysis (Figure 3), large time offsets (50 to 85 ms) were present between EC2 and CA3/dentate principal cells and between EC3 and CA1 pyramidal neurons (black arrows in Figure 4A). The group cross-correlograms of EC2-dentate gyrus (DG) and EC2-CA3 pairs showed the strongest theta modulation, whereas the magnitude of theta modulation was modest in EC3-CA1 pairs. Most of EC2-DG, EC2-CA3, and EC3-CA1 principal-principal neuron pairs had temporal offsets at [−60 to 0] ms or [60 to 120] ms, and only a minority of pairs had peaks at [0 to 30] ms. The group cross-correlogram and the distribution of temporal offsets between CA1 and EC5 principal cell pairs was essentially flat, whereas those of EC2-EC5 pairs and EC3-EC5 pairs were more strongly theta modulated (Figure 4A), indicating that EC5 principal neurons are more strongly controlled by intra-EC mechanisms than by the CA1 output during theta oscillations. Principal cells of EC2 and EC3 fired with time lags corresponding to preferences of opposite phases of the theta cycle (Figure 4A).

EC2 principal cell-EC2/3 interneuron pairs had small, whereas EC3 principal cell-EC2/3 interneuron pairs had large temporal offsets (gray arrows in Figure 4B), again in line with the theta LFP-unit analysis (Figure 3). EC2 principal cell-DG/CA3 interneuron pairs and EC3 principal cell-CA1 interneuron pairs also had large temporal offsets. Overall, these findings suggest that population activities in unidirectionally and monosynaptically connected layers/regions are significantly more delayed than would be expected from a simple drive-integrate model.

Rate versus Phase Relationship

Because the theta phase of spikes can vary as a function of the discharge frequency (Harris et al., 2002), we examined the relationship between these variables. The instantaneous firing rate of a given spike was taken as proportion to the number of spikes of that neuron within a 250 ms ($\sim$ two theta cycle) time window centered on that spike (1 spike/250 ms = $\sim$4 Hz; $\geq$10 spikes/250 ms = $\sim \geq$ 40 Hz; Harris et al., 2002). Firing rate changes were moderately correlated with the preferred phases of DG and CA3 principal neurons (<90°), without a detectable effect on the modulation depth (Figures 5 and S12). Firing rates had a relatively small effect on EC3 principal cells as a population and a large variability of phase preference was observed at higher rates. In contrast, as firing rate increased, EC2 and CA1 principal neurons advanced to progressively earlier phases (>150° phase shifts; Figure 5A curved arrows), and EC2 principal neurons also showed a decreasing magnitude of phase-locking with phase advancement.

In addition to sustained fast discharge, we also examined the phase preference of burst firing patterns (defined as < 6 ms interspike intervals; Figure S4; Ranck, 1973). In general, bursts tended to occupy similar theta phase as sustained fast-frequency spikes ($\geq$40 Hz) but in the case of EC2 and CA1 principal neurons burst probability had two small peaks (arrows in Figures 5B and S12B). Firing rate and bursting, in the frequency range similar to principal cells, marginally affected the interneuron's spiking phase (<30° shift; Figure S13). These analyses emphasize that treating all action potentials equally does not fully capture the proper relationship between spiking and theta phase because spike rate changes are associated with differential phase preferences in different layers/regions.

Phase Precession in the Hippocampus and EC

Hippocampal and EC principal neurons have been shown to discharge at progressively earlier phases of the theta cycle as

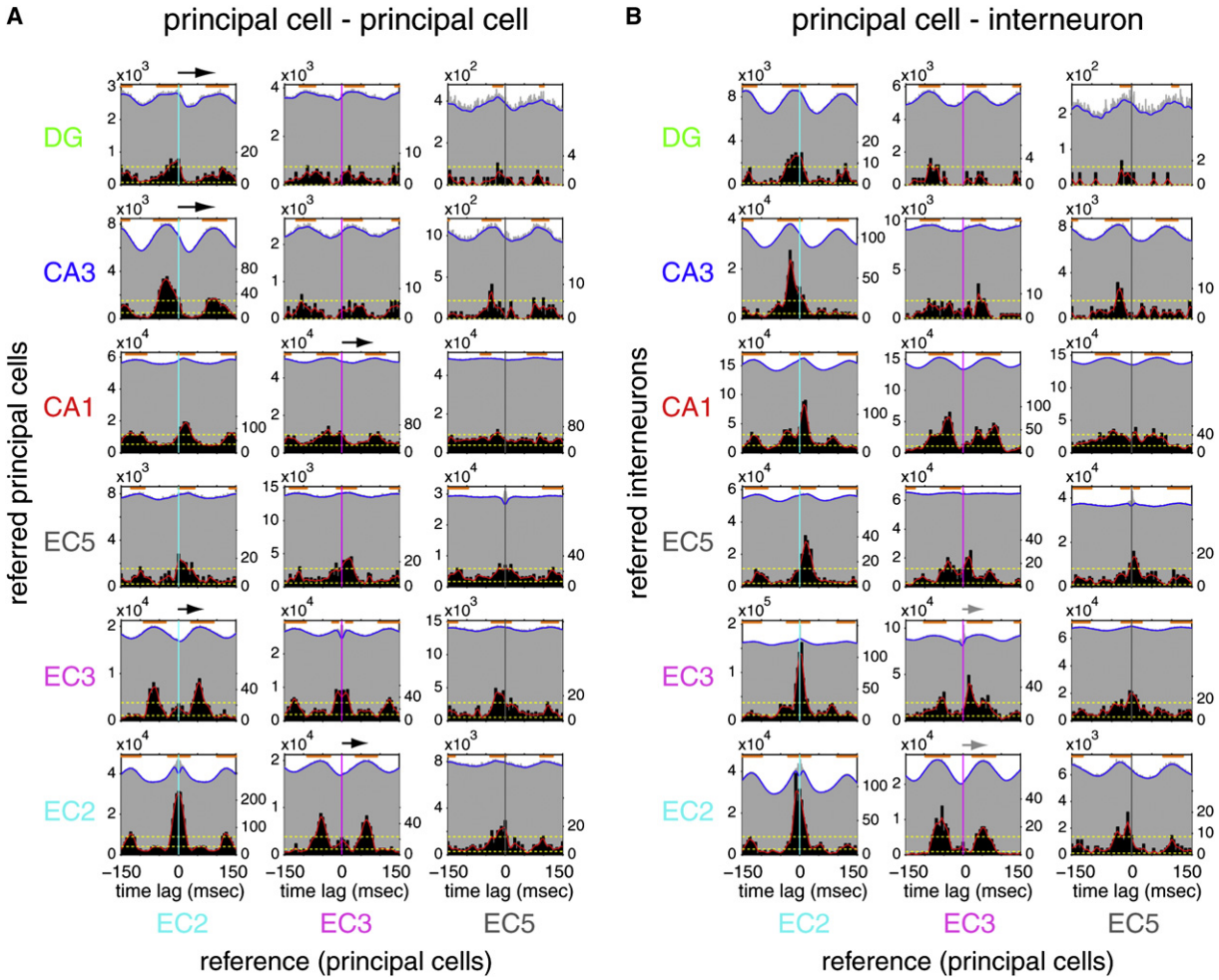

Figure 4. Temporal Relationship between Neuron Groups of Hippocampus and EC

(A) Temporal relationship of principal neurons across different regions. Time zero, spike time of the reference neuron. Grey histograms: group cross-correlograms of principal neuron pairs. Counts in cross-correlograms of all the pairs in each category were summed up. Orange lines above cross-correlograms show significant peak bins ($p < 0.001$) for group cross-correlograms. Blue line: smoothed group cross-correlograms. Y scale (left), spike counts of the referred neuron. Black histograms: distribution of temporal offsets (cross-correlogram peaks of significantly correlated neuron pairs; see Supplemental Experimental Procedures). Y scale (right), number of neuron pairs. Ninety-five percent confidence intervals (yellow broken lines) are applied to smoothed distributions of temporal offsets (red lines; see Supplemental Experimental Procedures). Arrows, time offsets between reference spike and peak activity of anatomically connected target neurons.

(B) Same as (A) but referred cells are putative interneurons. Time bin, 1 ms for group cross-correlograms; 5 ms for the distribution of temporal offsets.

the rat moves through the firing field of the neuron (O'Keefe and Recce, 1993; Skaggs et al., 1996; Hafting et al., 2008). In support of these previous observations, we also observed advancement of spike phase with position in both the hippocampus and EC (Figure 6). Hippocampal principal neurons in all subregions showed a robust phase precession slope (Figures 6H–6J), even at peak firing rates as low as 5 Hz. Occasionally, when multiple place fields were observed on the linear track, each field was associated with phase precession of spikes (Figure S14; Maurer et al., 2006a). In contrast, most EC cells had multiple firing fields or showed maintained spiking with low spatial coherence (Hafting et al., 2008; Supplemental Data) during large part of the travel. Distinct firing fields with large peak rates and high spatial coherence in EC were often but not always associated with phase precession of the spikes (Figures 6A–6G). Even within the same neuron, some fields showed robust phase precession, comparable to that of hippocampal neurons, while in other fields, spikes remained phase locked or no consistent phase-position relationship could be revealed (Figures 6A–6E). At recording positions, where neurons displayed grid-firing patterns in the open field (Hafting et al., 2005), multiple firing fields with associated phase precession were observed in the maze (Figure S14; Hafting et al., 2008).

The correlation between theta phase and the rat's position on the linear track was determined for each firing field with >0.7 spatial coherence at the phase rotation that gave the regression line with the largest explained variance (Hafting et al., 2008). Among EC cells, EC2 cells had the highest proportion of

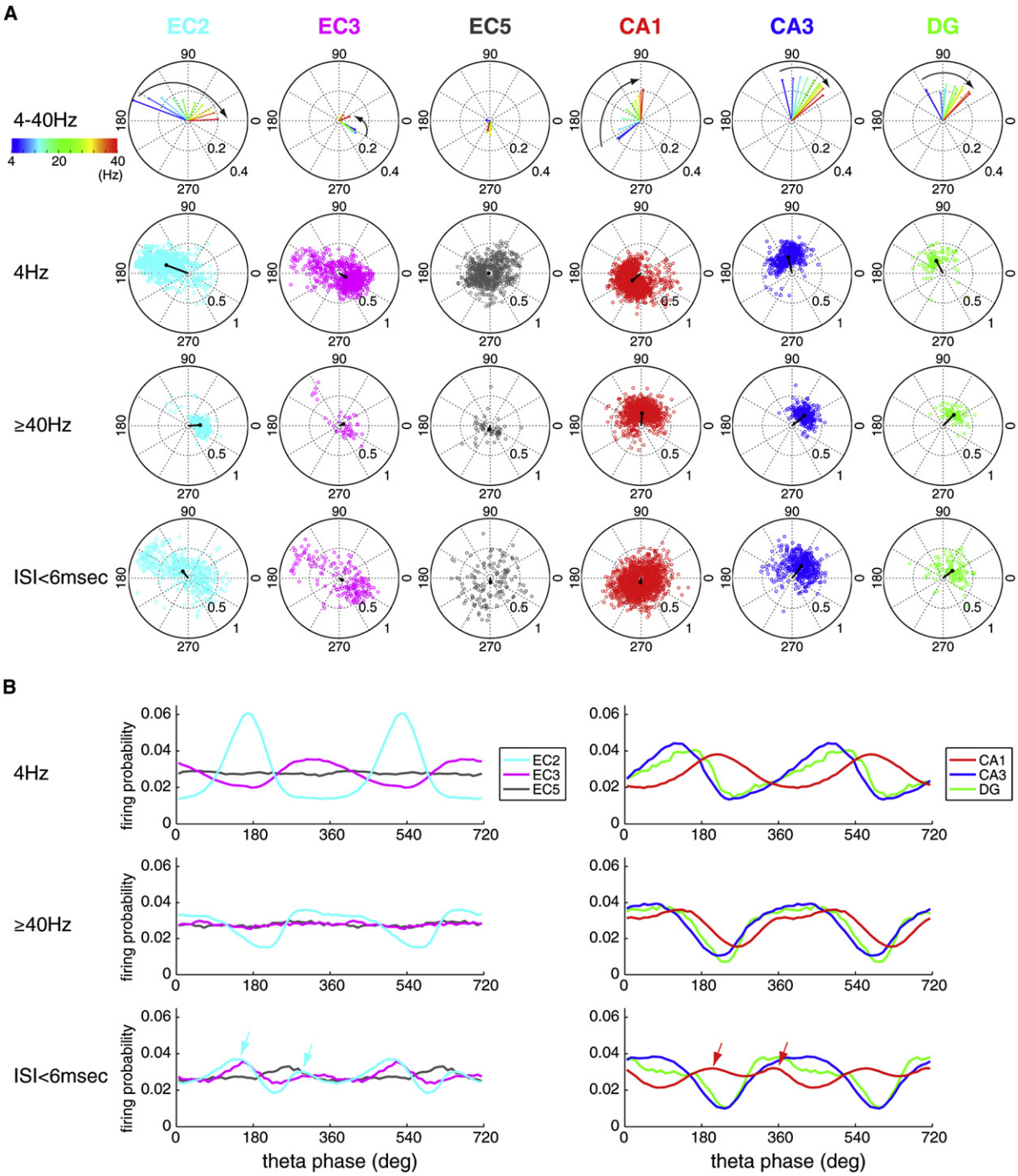

Figure 5. Relationship between Firing Rate and Theta Phase

(A) Top row, polar plots of group mean of preferred phase and mean resultant length as a function of instantaneous firing rate (color coded). Instantaneous rate was quantified for each spike in ten increments (1, 2, … or ≥10 spikes per 250 ms (two theta cycles), corresponding to 4, 8, 12,…, ≥40 Hz; Harris et al., 2002). Second and third rows show preferred phase and mean resultant length for each significantly modulated principal neuron at 4 and ≥40 Hz. Fourth row, same but for bursting spikes (interspike interval < 6 ms). Each circle is a single neuron. Black lines, group mean. Note the large and progressive shifts of preferred phase in EC2 and CA1 cells with rate increase. In each firing rate category, only neurons with significant theta modulation (at least 50 spikes in a given category and Rayleigh test, $p < 0.01$) are shown.

(B) Firing probability of principal neurons from different layers as a function of theta phase (as in Figures 3A and 3E), at different instantaneous frequencies (4 Hz, ≥40 Hz, bursting spikes, ISI < 6 ms). In each category, all neurons are included regardless of the significance of theta modulation. Note the large shift of active phase of EC2 and CA1 neurons between 4 Hz and ≥40 Hz of activity. Arrows in the bottom row indicate double peaks of bursting activity (ISI < 6 ms) in EC2 and CA1.

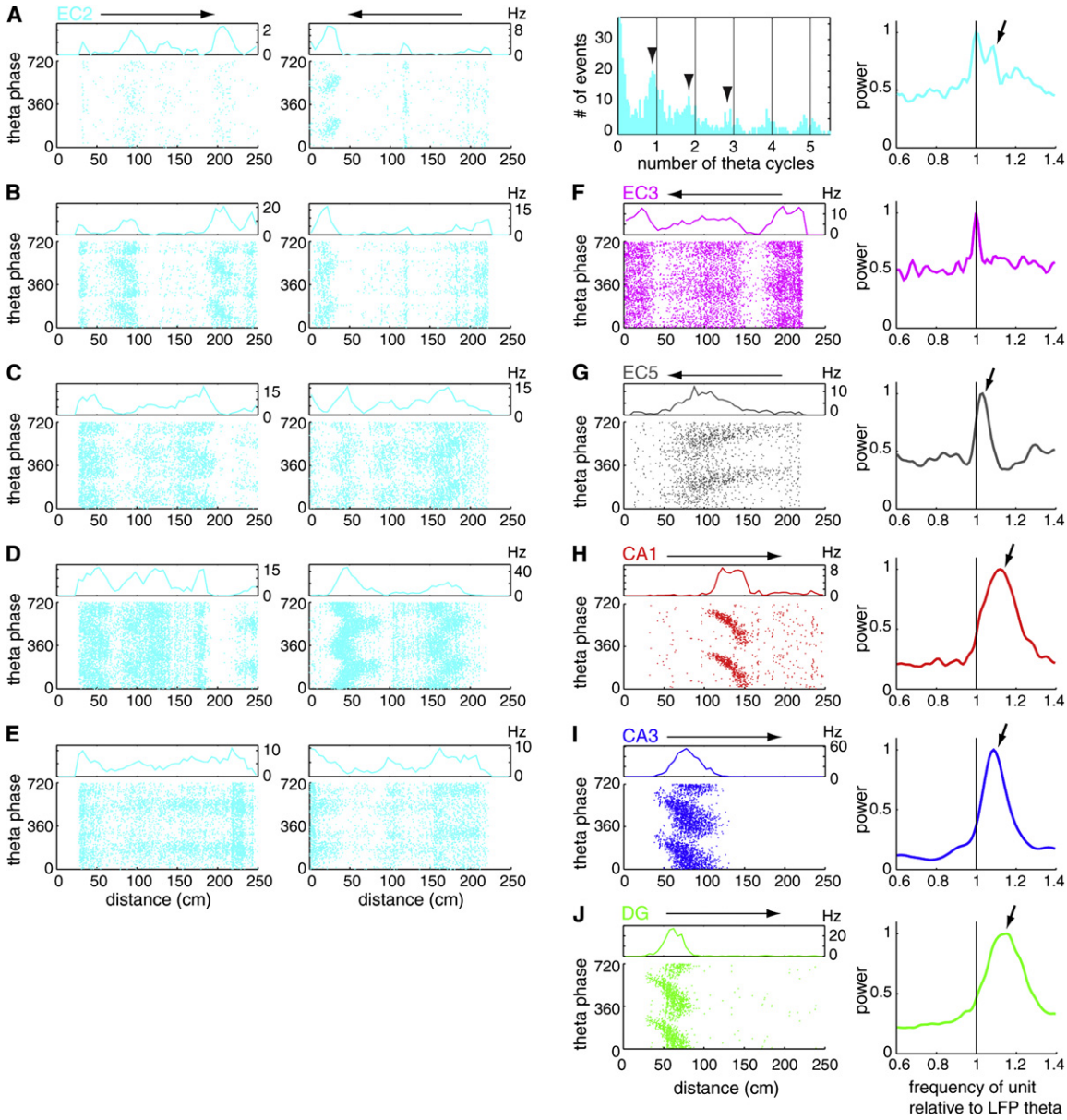

Figure 6. Examples of Phase Precessing EC and Hippocampal Neurons

(A) Theta phase related firing pattern of an EC2 neuron as a function of position on a linear track. Note the precession of spike phase between 5 and 40 cm on the leftward journey. Horizontal arrows above rate histograms represent the direction of travel. Spike phase autocorrelogram illustrates faster oscillatory activity of spikes relative to LFP theta (arrowheads, lines: multiples of 360°). Arrow on the phase spectrum (right; see Supplemental Data; Figure S17), obtained from leftward journeys, indicates an oscillation frequency of unit firing faster than that of the theta LFP (black line).

(B–D) Three further examples of phase precessing EC2 neurons and (E) a theta phase-locked EC2 neuron.

(F) EC3 cell with no consistent phase-position relationship and (G) phase precessing EC5 cell.

(H, I, and J) Example CA1, CA3 pyramidal neurons and granule cell.

(A–C) and (D–F) are from the same session. Reference theta is from EC3 for all neurons. Power spectra in the rightmost column were normalized by their peaks.

negatively correlated place fields, but neurons in all hippocampal regions had higher proportion of negatively correlated fields than EC2 (Figure 7A). We also calculated the mean spike phase shifts for all firing fields with >0.7 spatial coherence. Principal neurons in EC3, as a group, did not show phase changes with position within firing fields (see also Hafting et al., 2008). The mean phase shifts for neurons in other layers/regions were comparable (Figure S15).

In our data sets, only a minority of place fields of EC cells were associated with spatial coherence greater than 0.7 (a cutoff used in Hafting et al., 2008). Furthermore, the firing fields of many EC cells were difficult to identify (e.g., Figures 6A–6G and S14; see

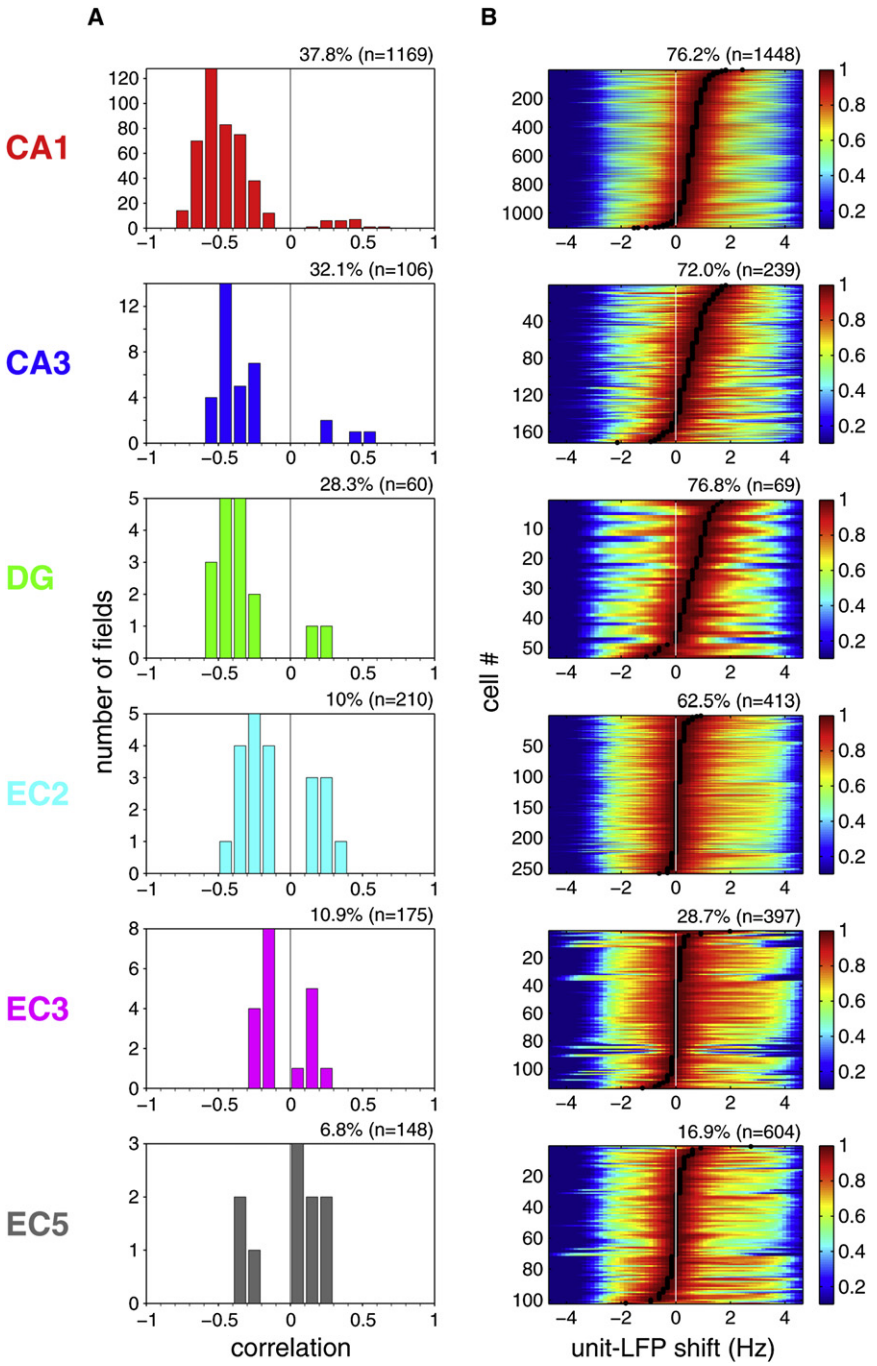

Figure 7. Phase Precession of EC and Hippocampal Neurons

(A) Distribution of the strength of phase precession of principal neurons in different regions/layers (correlation between phase and position; see Supplemental Data). Only firing fields with high spatial coherence (>0.7; Hafting et al., 2008) in the linear track are included (indicated as % fields, n; total number of place fields).

(B) Differences between oscillation frequencies of neuron firing and LFP theta, determined by computing the cross-correlogram of the spectra of the respective neuron and LFP (Geisler et al., 2007). Each color-coded row represents a single principal neuron, sorted by the magnitude of frequency shift (black dots) determined by the peak of cross-correlograms. Cross-correlograms were normalized by their peaks. Peak at 0 Hz indicates lack of phase precession. Only neurons with significant theta power in the linear track task are shown (expressed as % neurons, n; total number of neurons). For other behaviors, see Figures S16 and S18.

also Hafting et al., 2008), which limited our analysis to "good" firing fields. Assuming that all spikes carry signals to downstream targets, we performed two additional phase precession measurements, which did not require identification of place fields. In both calculations, we exploited the fact that for phase precession to be present, the neuron should oscillate faster than the reference LFP theta (O'Keefe and Recce, 1993; Maurer et al., 2006a; Geisler et al., 2007; Jeewajee et al., 2008). In the first analysis, the maximum of the cross-correlogram between the power spectra of neuronal spikes and LFP provided a quantitative measure of the oscillation frequency difference between single neurons and the concurrently recorded LFP theta (Geisler et al., 2007; Jeewajee et al., 2008). As shown in Figure 7B, the great majority of hippocampal principal cells and a smaller fraction of EC principal neurons oscillated faster (frequency shift >0) than the simultaneously recorded EC3 LFP theta on the linear track (O'Keefe and Recce, 1993; Hafting et al., 2008). Virtually identical results were obtained when local theta, instead of EC3 theta, was used as the reference signal (data not shown). Furthermore, the overall results were the same when data obtained from recordings in the linear track, open field, T maze, and rewarded wheel-running task were analyzed separately, with the smallest magnitude of the unit-LFP frequency shift present in the open field for all neuron types (Figure S16; Huxter et al., 2008). In addition, we introduced a novel method, the "spike phase spectrum" (SPS), to quantify phase precession (see Supplemental Data). By analogy to the power spectrum of spiking point process in time, we estimated a power spectrum of spiking point process in monotonically increasing continuous theta phase (Figure S17). Because the spikes are always referred to their own theta cycle in the SPS calculation, it is a reliable method for the quantification of spike-phase precession even when the frequency of theta cycles varies over time. The spike phase spectrum method (Figures 6A, 6F–6J, and S18) confirmed the phase precession results obtained by the unit

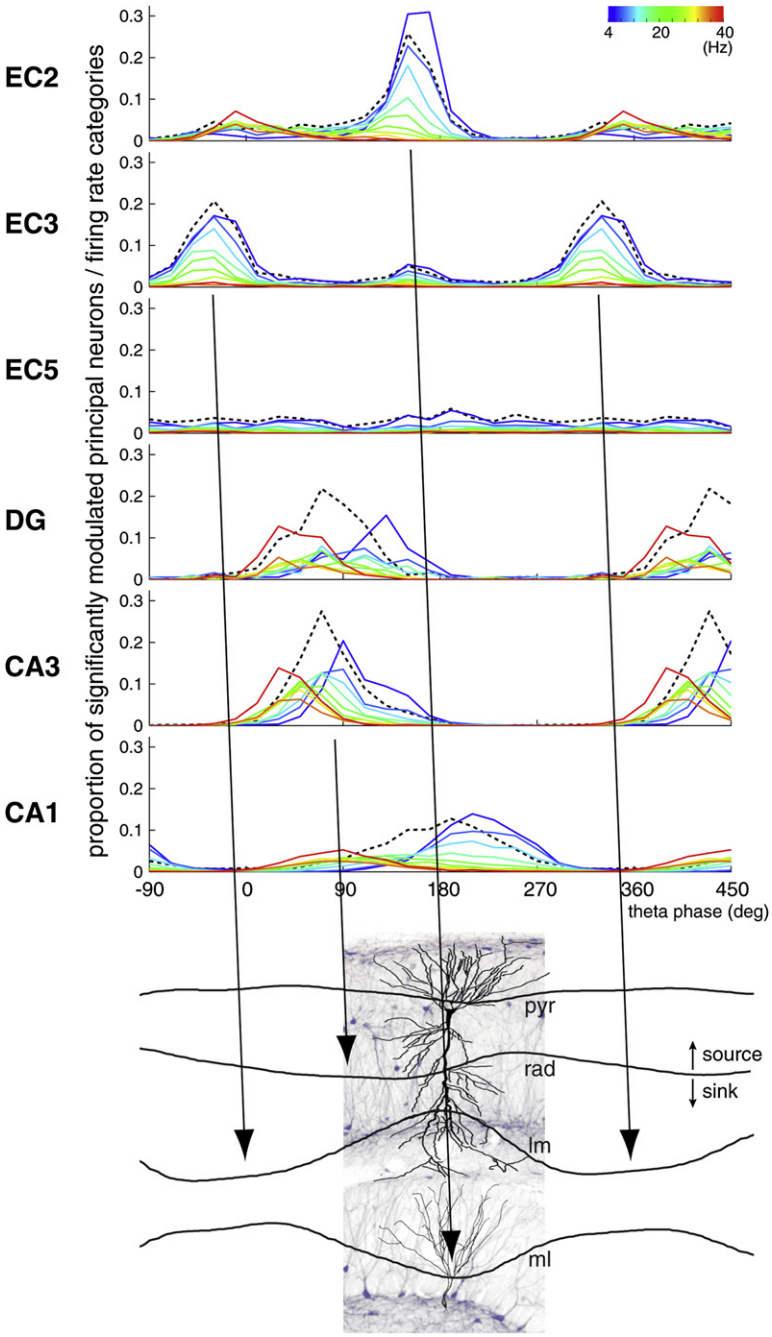

Figure 8. Temporal Relationship between Layer-/Region-Specific Firing Patterns and Theta Current Sinks in the Hippocampus

Top: distribution of preferred theta phase. The height of the histograms reflects the proportion of principal neurons significantly modulated in each firing rate category (as in Figure 5A; reference = EC3 theta). Black dashed line, population mean (as in Figure 3B). Instantaneous rate (color coded) was quantified for each spike in ten increments (1, 2, … or ≥10 spikes per 250 ms [~two theta cycles], corresponding to 4, 8, 12,…, ≥40 Hz; as in Figure 5). In each region and layer, most principal neurons are silent or fire at low rates, with only a minority of neurons discharging at high frequency at a given time (Figure S19). Bottom: current-source density (CSD) theta traces, taken from Montgomery et al. (2009), are superimposed on a histological section in the CA1-dentate gyrus axis, with highlighted pyramidal cell and granule cell. Note phase-reversed sinks in CA1 str. lacunosum-moleculare (lm) and dentate molecular layers (ml), and phase-shifted sink (relative to lm sink) in str. radiatum (rad). pyr, pyramidal layer. Arrows indicate the temporal (phase) offsets between the peak of population firing in upstream layers and the theta sinks in the target layers with the expected delays (based on axonal conduction velocity; 30° or ~10 ms). Note that while the population peak of an upstream layer correctly predicts the timing of the dendritic sink in its target layer, spiking activity in the downstream target population is substantially delayed.

versus LFP oscillation frequency comparison (Figure S16), and both methods expanded the quantification of phase precession obtained with the phase-position correlation analysis. These findings demonstrate that only a minority of principal cells in the EC show high spatial coherence and phase precession, while the majority of neurons keep a constant theta phase preference. The highest prevalence and strongest phase precession was observed in the CA1 region, whereas in the EC3, a major source of direct input to CA1, phase precessing neurons were exceptional.

DISCUSSION

Unexpectedly, we found that the temporal delays between population activities in successive stages of the EC-hippocampal loop were considerably longer during theta-associated behaviors than would be expected by axon conduction velocity, synaptic delay, and neuronal integration of feedforward excitatory inputs. Although the peak of population activity in an upstream structure corresponded well with the timing of dendritic excitation of downstream target neurons (current sinks; Figure 8) in the hippocampus, the discharge of the respective target populations was typically offset by a half theta cycle. These findings suggest that the theta dynamic allows for a considerable degree of independence of local circuit computation in the successive stages of the EC-hippocampal system (Figure 8), rather than imposing rapidly propagating activity across regions. In addition, our findings illustrate that lumping all cells of a given region into a "representative mean neuron" cannot provide sufficient description of neural communication in oscillatory systems.

EC Contribution to Theta LFP

A quantitative estimate for the excitatory effect of an upstream region during theta can be obtained by identifying the location and magnitude of the extracellular current sinks along the soma-dendritic domains in the target region and relating sinks to the discharge patterns of the upstream projection neurons.

The present results, combined with previous current-source density experiments, provide such information. The largest theta sinks in the hippocampus are present in CA1 str. lacunosum-moleculare and the midmolecular layer of the dentate gyrus, and these sinks are shifted by 90°–180° relative to each other (Figure 8; Buzsáki et al., 1986; Brankack et al., 1993; Montgomery et al., 2009). Since the stratum lacunosum-moleculare and the molecular layer are the major recipients of EC afferents, and because the spike propagation speed in these fiber pathways is relatively fast (0.6–3 m/s; Andersen et al., 1969; Empson and Heinemann, 1995), it is expected that the population output of EC neurons is followed by the respective sinks in the appropriate layers within an ~30° theta phase delay. We demonstrate here that the theta phases of the sinks in stratum lacunosum-moleculare and the molecular layer (Buzsáki et al., 1986; Brankack et al., 1993; Montgomery et al., 2009) are preceded by the maximum probability of discharge of EC3 and EC2 principal cells, respectively, with the expected delays (tilted arrows in Figure 8), indicating that a major source of these theta sinks in the hippocampus is the synchronous discharge of the respective EC neuronal populations. In summary, population behavior of EC neurons can provide an accurate description of both the spatial locations and timing of the theta current sinks they produce in the respective hippocampal layers (Figure 8).

EC2 principal (stellate) neurons have long been considered a key contributor to theta rhythm generation because they are endowed with intrinsic properties to oscillate at theta frequency, due mainly to the high density of HCN1 channels in these cells (Alonso and Llinás, 1989; Giocomo et al., 2007). In accordance with the biophysical and anatomical properties of stellate cells, EC2 principal neurons showed the strongest theta modulation of all neuron types (Figure 3) and theta waves were reversed between layers I and III (Mitchell and Ranck, 1980; Alonso and García-Austt, 1987; Chrobak and Buzsáki, 1998). Most EC2 interneurons and a large proportion of EC3 interneurons fired in phase with EC2 stellate cells, the latter neurons likely exciting both interneuron populations directly. We hypothesize that the stellate-yoked interneurons in EC3 exert strong inhibition on EC3 principal cells, allowing them to discharge mainly when least inhibited within the theta cycle.

The peak discharge of EC2 and EC3 principal neuron populations at the opposite phases of the theta waves were followed by the largest amplitude sinks in the dentate molecular layer and the CA1 str. lacunosum-moleculare, respectively. However, the theta phases of the maximal discharge of EC2 and EC3 populations and associated depolarization of the respective dendritic domains in the hippocampus cannot fully account for population activity in the hippocampus due to the long delays between dendritic depolarization and output spiking of DG, CA3 and CA1 neurons.

Population Dynamics in the Hippocampus and EC: Delays during Theta Oscillations

A general assumption in neuronal network models is that increased firing rate of a target population is the result of an increased discharge of upstream afferent population. In agreement with such a feed-forward "synfire chain" model (Abeles, 1991), neurons in the CA3-CA1-subiculum-EC axis fire sequentially during sharp waves, and interregional delays can be explained by axonal conduction velocity, synaptic delays and passive temporal integration by neurons in downstream regions/layers (Figure S2; Chrobak and Buzsáki, 1994). By analogy, it has been tacitly assumed that similar integration rules govern information transfer during theta oscillations (Leung, 1984; cf., Bland 1986; Buzsáki, 2002). In line with this view, it has been suggested that hippocampal place cells (O'Keefe and Dostrovsky, 1971) arise from the spatial and temporal convergence of EC grid cells (Moser et al., 2008) and that the phase precession of hippocampal place cells is inherited from the precessing grid cells (Maurer and McNaughton, 2007; Molter and Yamaguchi, 2008; Hafting et al., 2008). However, the long delays between the upstream EC population activity and the spike discharge of hippocampal neurons within theta cycles (Figure 8) cannot be fully explained by a simple integration model.

The phase-time relationships of the fast-firing minority of neurons may provide a partial explanation for the long delays between dendritic sinks and spike timing. Under this hypothesis, the fast-firing minority exerts a disproportionally larger impact on downstream neurons, while the effect of the slow firing majority is somehow filtered out. Accordingly, the most active EC2 principal cells (e.g., grid cells) would discharge their target DG and CA3 neurons after a short delay (30–60 degrees; compare the preferred phases of the high-firing rate groups, marked by hot colors in Figure 8). In turn, the fast firing CA3 neurons would discharge the fast firing CA1 minority after a short delay (30–60 degrees; hot colors in Figure 8), perhaps "boosted" by prior EC3 activation. Synaptic facilitation (Miles and Wong, 1986) and/or efficient temporal integration of spatially confined dendritic inputs from coherently active small group of cells (Losonczy et al., 2008) might explain how the fast firing minority can "drive" downstream neurons more effectively than the slow firing majority. However, under this hypothesis, the driving force for the slow firing majority downstream neurons (Figure 8, cold colors; see also Figure S19) remains unaccounted for without further mechanisms.

Another explanation for the long delays involves feed-forward excitation of interneurons (Buzsáki, 1984), which can decelerate the rate of depolarization and delay the spiking of the inhibited principal cells. However, this mechanism can account for only 10 to 20 ms delays (commensurate with the time constant of the $GABA_A$ receptor). Furthermore, our recordings were mainly confined to the cell body layers and, therefore, sampled mostly basket and chandelier cells. Although these interneurons are well suited for feed-forward inhibition since they are directly innervated by the entorhinal afferents and mediate perisomatic inhibition (Kiss et al., 1996), their activity largely paralleled the behavior of their respective principal cells (Figures 3, 4, S11, and S13), instead of responding robustly after the excitatory volley from the EC. However, there are numerous other interneuron classes in the hippocampus with variable theta phase preferences (Somogyi and Klausberger, 2005), which may not have been included in our data set and may significantly delay the depolarizing effect of the EC inputs. Exploring other complex interactions, such as synaptic facilitation and depression, between principal cells and the multiple interneuron families during theta (Traub et al., 2004; Klausberger and Somogyi,

2008; Fujisawa et al., 2008; Diba and Buzsáki, 2008) is an important task for future experiments. In addition, the synaptic interactions between trisynaptic and temporoammonic pathways (Remondes and Schuman, 2002; Ang et al., 2005) and pathway-specific synaptic modulation (Otmakhova and Lisman, 1999) may also contribute to the long delays observed in our experiments. Finally, the role of the lateral EC, another major input to the hippocampus, in the temporal coordination of hippocampal neurons (Hargreaves et al., 2005) should also be addressed.

Theta Oscillations Support Self-Generated Assemblies

In agreement with a recent study, EC2 principal neurons ("one-dimensional grid cells"; Hafting et al., 2008) showed phase precession (Figures 6A–6D). In our data set, such neurons constituted a minority of EC2 cells, while the majority of EC2 cells fired at a relatively low rate and were strongly phase-locked to the theta cycle. It is feasible that the output of fast firing and phase advancing EC2 grid cells is selectively integrated by target granule and CA3 pyramidal cells (Molter and Yamaguchi, 2008; Hafting et al., 2008; Moser et al., 2008), as discussed above. Yet, it remains unclear how the EC2 input can support phase precession in the CA1 region, given that neurons in EC3 did not show phase precession (see also Hafting et al., 2008).

To interpret both the observed long delays between successive stages of the EC-hippocampal system and the higher prevalence of phase precessing neurons in the hippocampus, we hypothesize that the long delays and phase precession reflect the same or interrelated mechanisms and that spikes at the earlier theta phase arise mainly from local circuit interactions. Under this hypothesis, we consider three types of activity patterns in the target hippocampal neurons. The first pattern is subthreshold depolarization ("silent" neurons) by the EC afferents. Given the extensive divergence of EC afferents (Steward, 1976; cf. Amaral and Witter, 1989), discharge of EC2 and EC3 principal cells is expected to induce subthreshold depolarization in the dendrites of large numbers of hippocampal neurons, reflected by extracellular current sinks. The second pattern is represented by a suprathreshold but weakly activated neuron group ("slow" firing cells) which discharge at the peak of dendritic depolarization (sink), brought about by the EC input. A third pattern is displayed by a small fraction of highly active neurons, which fire multiple spikes (spike trains and bursts) transiently in each theta cycle. Each neuron can belong to one of the above firing categories at different moments but the proportions of silent, slow firing and fast discharging neurons should remain similar in successive theta cycles.

The temporal evolution of spiking patterns during spatial behavior may help to understand the origin of spike trains. For example, the arrival of the rat at the beginning of the place field of a CA1 neuron is signaled by the occurrence of a single spike on the late ascending phase of the local theta wave. Given that the EC3 principal cell population fire maximally at this phase (Figure 3), the EC3 input may be responsible for the CA1 spikes that occur at this late phase. As the animal moves into the field, firing rate increases and the additional spikes occur at progressively earlier phases (O'Keefe and Recce, 1993). In the middle of the field, CA1 spikes fire maximally at the trough of the theta cycle, i.e., at the phase where EC3 output is at its minimum. Similarly, the spiking onset of DG/CA3 place cells corresponds to the maximum discharge of the EC2 population and the associated sink in the molecular layer (Montgomery et al., 2009), but the preferred discharge phase of DG/CA3 neuron population cannot be explained by the population output of EC2 neurons. We hypothesize that higher frequency spiking at the earlier theta phases arise mainly from intrahippocampal circuits. Under this hypothesis, hippocampal neurons, initially discharged by the EC, begin to interact with each other in the form of transient oscillating assemblies. We propose that the phase interference occurs between the majority of weakly depolarized neurons, whose membrane oscillations are coherent with theta LFP, and a faster oscillating assembly of principal cells and dedicated interneurons (Maurer et al., 2006b; Geisler et al., 2007). This is in contrast to models based on the interference of global theta and single neuron oscillators (O'Keefe and Recce, 1993; Kamondi et al., 1998; Harris et al., 2002; Mehta et al., 2002; Lengyel et al., 2003; Burgess et al., 2007; Hasselmo, 2007, 2008; Jeewajee et al., 2008). In our hypothetical model, a major role of the EC input is to select a subset of hippocampal neurons, which begin to interact with each other and additionally recruit cells in the form of a transient, self-sustained activity (Tsodyks et al., 1996; Wallenstein and Hasselmo, 1997; Hasselmo et al., 2002; Jensen and Lisman, 2005; Dragoi and Buzsáki, 2006). From this perspective, an important function of the theta cycle is to allocate sufficient time for local computation before the results are transmitted to downstream regions.

EXPERIMENTAL PROCEDURES

Five rats were implanted with movable, multiple-site silicon probes in the dorsal hippocampus and the dorsocaudal medial EC (EC; Fujisawa et al., 2008; Hafting et al., 2005). They were trained in four different testing environments. Neurophysiological signals were acquired continuously and analyzed offline. Detailed methods of behavioral testing, recording setup and data analyses are available as Supplemental Data.

SUPPLEMENTAL DATA

Supplemental Data include 19 Figures, 1 Table, and Supplemental Experimental Procedures and can be found with this article online at http://www.neuron.org/supplemental/S0896-6273(09)00673-4.

ACKNOWLEDGMENTS

We thank A. Amarasingham, K. Diba, S. Fujisawa, C. Geisler, A. Grosmark, S.M. Montgomery, S. Ozen, J. Patel, P. Quilichini, S. Sakata, E. Stark, D. Sullivan, and D. Robbe for valuable discussions and comments on the manuscript. Supported by National Institutes of Health (NS034994; MH54671), National Science Foundation (SBE 0542013), the J.D. McDonnell Foundation, Uehara Memorial Foundation, Astellas Foundation for Research on Metabolic Disorders, Japan Society for the Promotion of Science, and the Robert Leet & Clara Guthrie Patterson Trust.

Accepted: August 26, 2009
Published: October 28, 2009

REFERENCES

Abeles, M. (1991). Corticonics: Neural Circuits of the Cerebral Cortex (Cambridge: Cambridge University Press).

Alonso, A., and García-Austt, E. (1987). Neuronal sources of theta rhythm in the entorhinal cortex of the rat. I. Laminar distribution of theta field potentials. Exp. Brain Res. *67*, 493–501.

Alonso, A., and Llinás, R.R. (1989). Subthreshold Na+-dependent theta-like rhythmicity in stellate cells of entorhinal cortex layer II. Nature *342*, 175–177.

Amaral, D.G., and Witter, M.P. (1989). The three-dimensional organization of the hippocampal formation: a review of anatomical data. Neuroscience *31*, 571–591.

Amaral, D., and Lavenex, P. (2007). Hippocampal Neuroanatomy. In The Hippocampus Book, P. Andersen, R. Morris, D. Amaral, T. Bliss, and J. O'Keefe, eds. (New York: Oxford University Press), pp. 37–114.

Andersen, P., Bliss, T.V., Lømo, T., Olsen, L.I., and Skrede, K.K. (1969). Lamellar organization of hippocampal excitatory pathways. Acta Physiol. Scand. *76*, 4A–5A.

Ang, C.W., Carlson, G.C., and Coulter, D.A. (2005). Hippocampal CA1 circuitry dynamically gates direct cortical inputs preferentially at theta frequencies. J. Neurosci. *25*, 9567–9580.

Barthó, P., Hirase, H., Monconduit, L., Zugaro, M., Harris, K.D., and Buzsáki, G. (2004). Characterization of neocortical principal cells and interneurons by network interactions and extracellular features. J. Neurophysiol. *92*, 600–608.

Bland, B.H. (1986). The physiology and pharmacology of hippocampal formation theta rhythms. Prog. Neurobiol. *26*, 1–54.

Bragin, A., Jandó, G., Nadasdy, Z., Hetke, J., Wise, K., and Buzsáki, G. (1995). Gamma (40–100 Hz) oscillation in the hippocampus of the behaving rat. J. Neurosci. *15*, 47–60.

Brankack, J., Stewart, M., and Fox, S.E. (1993). Current source density analysis of the hippocampal theta rhythm: associated sustained potentials and candidate synaptic generators. Brain Res. *615*, 310–327.

Brun, V.H., Otnass, M.K., Molden, S., Steffenach, H.A., Witter, M.P., Moser, M.B., and Moser, E.I. (2002). Place cells and place recognition maintained by direct entorhinal-hippocampal circuitry. Science *296*, 2243–2246.

Burgess, N., Barry, C., and O'Keefe, J. (2007). An oscillatory interference model of grid cell firing. Hippocampus *17*, 801–812.

Buzsáki, G. (1984). Feed-forward inhibition in the hippocampal formation. Prog. Neurobiol. *22*, 131–153.

Buzsáki, G. (2002). Theta oscillations in the hippocampus. Neuron *33*, 325–340.

Buzsáki, G. (2006). Rhythms of the Brain (New York: Oxford University Press).

Buzsáki, G., Leung, L.W., and Vanderwolf, C.H. (1983). Cellular bases of hippocampal EEG in the behaving rat. Brain Res. *287*, 139–171.

Buzsáki, G., Czopf, J., Kondakor, I., and Kellenyi, L. (1986). Laminar distribution of hippocampal rhythmic slow activity (RSA) in the behaving rat: current-source density analysis, effects of urethane and atropine. Brain Res. *365*, 125–137.

Chrobak, J.J., and Buzsáki, G. (1994). Selective activation of deep layer (V-VI) retrohippocampal cortical neurons during hippocampal sharp waves in the behaving rat. J. Neurosci. *14*, 6160–6170.

Chrobak, J.J., and Buzsáki, G. (1996). High-frequency oscillations in the output networks of the hippocampal-entorhinal axis of the freely behaving rat. J. Neurosci. *16*, 3056–3066.

Chrobak, J.J., and Buzsáki, G. (1998). Gamma oscillations in the entorhinal cortex of the freely behaving rat. J. Neurosci. *18*, 388–398.

Constantinidis, C., Williams, G.V., and Goldman-Rakic, P.S. (2002). A role for inhibition in shaping the temporal flow of information in prefrontal cortex. Nat. Neurosci. *5*, 175–180.

Csicsvari, J., Hirase, H., Czurko, A., and Buzsáki, G. (1998). Reliability and state dependence of pyramidal cell-interneuron synapses in the hippocampus: an ensemble approach in the behaving rat. Neuron *21*, 179–189.

Csicsvari, J., Hirase, H., Czurko, A., Mamiya, A., and Buzsáki, G. (1999). Oscillatory coupling of hippocampal pyramidal cells and interneurons in the behaving rat. J. Neurosci. *19*, 274–287.

Diba, K., and Buzsáki, G. (2008). Hippocampal network dynamics constrain the time lag between pyramidal cells across modified environments. J. Neurosci. *28*, 13448–13456.

Dragoi, G., and Buzsáki, G. (2006). Temporal encoding of place sequences by hippocampal cell assemblies. Neuron *50*, 145–157.

Empson, R.M., and Heinemann, U. (1995). The perforant path projection to hippocampal area CA1 in the rat hippocampal-entorhinal cortex combined slice. J. Physiol. *484*, 707–720.

Fox, S.E. (1989). Membrane potential and impedance changes in hippocampal pyramidal cells during theta rhythm. Exp. Brain Res. *77*, 283–294.

Frank, L.M., Brown, E.N., and Wilson, M.A. (2001). A comparison of the firing properties of putative excitatory and inhibitory neurons from CA1 and the entorhinal cortex. J. Neurophysiol. *86*, 2029–2040.

Freund, T.F., and Buzsáki, G. (1996). Interneurons of the hippocampus. Hippocampus *6*, 347–470.

Fujisawa, S., Amarasingham, A., Harrison, M.T., and Buzsáki, G. (2008). Behavior-dependent short-term assembly dynamics in the medial prefrontal cortex. Nat. Neurosci. *11*, 823–833.

Geisler, C., Robbe, D., Zugaro, M., Sirota, A., and Buzsáki, G. (2007). Hippocampal place cell assemblies are speed-controlled oscillators. Proc. Natl. Acad. Sci. USA *104*, 8149–8154.

Giocomo, L.M., Zilli, E.A., Fransen, E., and Hasselmo, M.E. (2007). Temporal frequency of subthreshold oscillations scales with entorhinal grid cell field spacing. Science *315*, 1719–1722.

Grastyán, E., Lissák, K., Madarász, I., and Donhoffer, H. (1959). Hippocampal electrical activity during the development of conditioned reflexes. Electroencephalogr. Clin. Neurophysiol. *11*, 409–430.

Hargreaves, E.L., Rao, G., Lee, I., and Knierim, J.J. (2005). Major dissociation between medial and lateral entorhinal input to dorsal hippocampus. Science *308*, 1792–1794.

Hafting, T., Fyhn, M., Molden, S., Moser, M.B., and Moser, E.I. (2005). Microstructure of a spatial map in the entorhinal cortex. Nature *436*, 801–806.

Hafting, T., Fyhn, M., Bonnevie, T., Moser, M.B., and Moser, E.I. (2008). Hippocampus-independent phase precession in entorhinal grid cells. Nature *453*, 1248–1252.

Harris, K.D., Henze, D.A., Hirase, H., Leinekugel, X., Dragoi, G., Czurko, A., and Buzsáki, G. (2002). Spike train dynamics predicts theta-related phase precession in hippocampal pyramidal cells. Nature *417*, 738–741.

Hasselmo, M.E. (2005). What is the function of hippocampal theta rhythm?—Linking behavioral data to phasic properties of field potential and unit recording data. Hippocampus *15*, 936–949.

Hasselmo, M.E. (2007). Arc length coding by interference of theta frequency oscillations may underlie context-dependent hippocampal unit data and episodic memory function. Learn. Mem. *14*, 782–794.

Hasselmo, M.E. (2008). Grid cell mechanisms and function: contributions of entorhinal persistent spiking and phase resetting. Hippocampus *18*, 1213–1229.

Hasselmo, M.E., Bodelón, C., and Wyble, B.P. (2002). A proposed function for hippocampal theta rhythm: separate phases of encoding and retrieval enhance reversal of prior learning. Neural Comput. *14*, 793–817.

Holmes, J.E., and Adey, W.R. (1960). Electrical activity of the entorhinal cortex during conditioned behavior. Am. J. Physiol. *199*, 741–744.

Huerta, P.T., and Lisman, J.E. (1995). Bidirectional synaptic plasticity induced by a single burst during cholinergic theta oscillation in CA1 in vitro. Neuron *15*, 1053–1063.

Huxter, J.R., Senior, T.J., Allen, K., and Csicsvari, J. (2008). Theta phase-specific codes for two-dimensional position, trajectory and heading in the hippocampus. Nat. Neurosci. *11*, 587–594.

Isomura, Y., Sirota, A., Ozen, S., Montgomery, S., Mizuseki, K., Henze, D.A., and Buzsáki, G. (2006). Integration and segregation of activity in entorhinal-hippocampal subregions by neocortical slow oscillations. Neuron *52*, 871–882.

Jeewajee, A., Barry, C., O'Keefe, J., and Burgess, N. (2008). Grid cells and theta as oscillatory interference: electrophysiological data from freely moving rats. Hippocampus *18*, 1175–1185.

Jensen, O., and Lisman, J.E. (2005). Hippocampal sequence-encoding driven by a cortical multi-item working memory buffer. Trends Neurosci. *28*, 67–72.

Kamondi, A., Acsady, L., Wang, X.J., and Buzsáki, G. (1998). Theta oscillations in somata and dendrites of hippocampal pyramidal cells in vivo: activity-dependent phase-precession of action potentials. Hippocampus *8*, 244–261.

Kiss, J., Buzsáki, G., Morrow, J.S., Glantz, S.B., and Leranth, C. (1996). Entorhinal cortical innervation of parvalbumin-containing neurons (Basket and Chandelier cells) in the rat Ammon's horn. Hippocampus *6*, 239–246.

Klausberger, T., and Somogyi, P. (2008). Neuronal diversity and temporal dynamics: the unity of hippocampal circuit operations. Science *321*, 53–57.

Kocsis, B., Bragin, A., and Buzsáki, G. (1999). Interdependence of multiple theta generators in the hippocampus: a partial coherence analysis. J. Neurosci. *19*, 6200–6212.

Konopacki, J., MacIver, M.B., Bland, B.H., and Roth, S.H. (1987). Carbachol-induced EEG 'theta' activity in hippocampal brain slices. Brain Res. *405*, 196–198.

Lengyel, M., Szatmary, Z., and Erdi, P. (2003). Dynamically detuned oscillations account for the coupled rate and temporal code of place cell firing. Hippocampus *13*, 700–714.

Leung, L.W. (1984). Model of gradual phase shift of theta rhythm in the rat. J. Neurophysiol. *52*, 1051–1065.

Losonczy, A., Makara, J.K., and Magee, J.C. (2008). Compartmentalized dendritic plasticity and input feature storage in neurons. Nature *452*, 436–441.

Markram, H., Toledo-Rodriguez, M., Wang, Y., Gupta, A., Silberberg, G., and Wu, C. (2004). Interneurons of the neocortical inhibitory system. Nat. Rev. Neurosci. *5*, 793–807.

Maurer, A.P., Cowen, S.L., Burke, S.N., Barnes, C.A., and McNaughton, B.L. (2006a). Organization of hippocampal cell assemblies based on theta phase precession. Hippocampus *16*, 785–794.

Maurer, A.P., Cowen, S.L., Burke, S.N., Barnes, C.A., and McNaughton, B.L. (2006b). Phase precession in hippocampal interneurons showing strong functional coupling to individual pyramidal cells. J. Neurosci. *26*, 13485–13492.

Maurer, A.P., and McNaughton, B.L. (2007). Network and intrinsic cellular mechanisms underlying theta phase precession of hippocampal neurons. Trends Neurosci. *30*, 325–333.

Mehta, M.R., Lee, A.K., and Wilson, M.A. (2002). Role of experience and oscillations in transforming a rate code into a temporal code. Nature *417*, 741–746.

Miles, R., and Wong, R.K. (1986). Excitatory synaptic interactions between CA3 neurones in the guinea-pig hippocampus. J. Physiol. *373*, 397–418.

Mitchell, S.J., and Ranck, J.B., Jr. (1980). Generation of theta rhythm in medial entorhinal cortex of freely moving rats. Brain Res. *189*, 49–66.

Mizumori, S.J., Perez, G.M., Alvarado, M.C., Barnes, C.A., and McNaughton, B.L. (1990). Reversible inactivation of the medial septum differentially affects two forms of learning in rats. Brain Res. *528*, 12–20.

Molter, C., and Yamaguchi, Y. (2008). Entorhinal theta phase precession sculpts dentate gyrus place fields. Hippocampus *18*, 919–930.

Montgomery, S.M., Sirota, A., and Buzsáki, G. (2008). Theta and gamma coordination of hippocampal networks during waking and rapid eye movement sleep. J. Neurosci. *28*, 6731–6741.

Montgomery, S.M., Betancur, M.I., and Buzsáki, G. (2009). Behavior-dependent coordination of multiple theta dipoles in the hippocampus. J. Neurosci. *29*, 1381–1394.

Moser, E.I., Kropff, E., and Moser, M.B. (2008). Place cells, grid cells, and the brain's spatial representation system. Annu. Rev. Neurosci. *31*, 69–89.

O'Keefe, J., and Dostrovsky, J. (1971). The hippocampus as a spatial map. Preliminary evidence from unit activity in the freely-moving rat. Brain Res. *34*, 171–175.

O'Keefe, J., and Recce, M.L. (1993). Phase relationship between hippocampal place units and the EEG theta rhythm. Hippocampus *3*, 317–330.

O'Keefe, J., and Burgess, N. (2005). Dual phase and rate coding in hippocampal place cells: theoretical significance and relationship to entorhinal grid cells. Hippocampus *15*, 853–866.

Orban, G., Kiss, T., and Erdi, P. (2006). Intrinsic and synaptic mechanisms determining the timing of neuron population activity during hippocampal theta oscillation. J. Neurophysiol. *96*, 2889–2904.

Otmakhova, N.A., and Lisman, J.E. (1999). Dopamine selectively inhibits the direct cortical pathway to the CA1 hippocampal region. J. Neurosci. *19*, 1437–1445.

Pastalkova, E., Itskov, V., Amarasingham, A., and Buzsáki, G. (2008). Internally generated cell assembly sequences in the rat hippocampus. Science *321*, 1322–1327.

Pavlides, C., Greenstein, Y.J., Grudman, M., and Winson, J. (1988). Long-term potentiation in the dentate gyrus is induced preferentially on the positive phase of theta-rhythm. Brain Res. *439*, 383–387.

Petsche, H., Stumpf, C., and Gogolak, G. (1962). The significance of the rabbit's septum as a relay station between the midbrain and the hippocampus. I. The control of hippocampus arousal activity by the septum cells. Electroencephalogr. Clin. Neurophysiol. *14*, 202–211.

Ranck, J.B., Jr. (1973). Studies on single neurons in dorsal hippocampal formation and septum in unrestrained rats. I. Behavioral correlates and firing repertoires. Exp. Neurol. *41*, 461–531.

Remondes, M., and Schuman, E.M. (2002). Direct cortical input modulates plasticity and spiking in CA1 pyramidal neurons. Nature *416*, 736–740.

Rotstein, H.G., Pervouchine, D.D., Acker, C.D., Gillies, M.J., White, J.A., Buhl, E.H., Whittington, M.A., and Kopell, N. (2005). Slow and fast inhibition and an H-current interact to create a theta rhythm in a model of CA1 interneuron network. J. Neurophysiol. *94*, 1509–1518.

Siapas, A.G., Lubenov, E.V., and Wilson, M.A. (2005). Prefrontal phase locking to hippocampal theta oscillations. Neuron *46*, 141–151.

Sirota, A., Montgomery, S., Fujisawa, S., Isomura, Y., Zugaro, M., and Buzsáki, G. (2008). Entrainment of neocortical neurons and gamma oscillations by the hippocampal theta rhythm. Neuron *60*, 683–697.

Skaggs, W.E., McNaughton, B.L., Wilson, M.A., and Barnes, C.A. (1996). Theta phase precession in hippocampal neuronal populations and the compression of temporal sequences. Hippocampus *6*, 149–172.

Soltesz, I., and Deschénes, M. (1993). Low- and high-frequency membrane potential oscillations during theta activity in CA1 and CA3 pyramidal neurons of the rat hippocampus under ketamine-xylazine anesthesia. J. Neurophysiol. *70*, 97–116.

Somogyi, P., and Klausberger, T. (2005). Defined types of cortical interneurone structure space and spike timing in the hippocampus. J. Physiol. *562*, 9–26.

Steward, O. (1976). Topographic organization of the projections from the entorhinal area to the hippocampal formation of the rat. J. Comp. Neurol. *167*, 285–314.

Steward, O., and Scoville, S.A. (1976). Cells of origin of entorhinal cortical afferents to the hippocampus and fascia dentata of the rat. J. Comp. Neurol. *169*, 347–370.

Stewart, M., and Fox, S.E. (1990). Do septal neurons pace the hippocampal theta rhythm? Trends Neurosci. *13*, 163–168.

Stewart, M., Quirk, G.J., Barry, M., and Fox, S.E. (1992). Firing relations of medial entorhinal neurons to the hippocampal theta rhythm in urethane anesthetized and walking rats. Exp. Brain Res. *90*, 21–28.

Traub, R.D., Bibbig, A., Lebeau, F.E., Buhl, E.H., and Whittington, M.A. (2004). Cellular mechanisms of neuronal population oscillations in the hippocampus in vitro. Annu. Rev. Neurosci. *27*, 247–278.

Tsodyks, M.V., Skaggs, W.E., Sejnowski, T.J., and McNaughton, B.L. (1996). Population dynamics and theta rhythm phase precession of hippocampal place cell firing: a spiking neuron model. Hippocampus *6*, 271–280.

Vanderwolf, C.H. (1969). Hippocampal electrical activity and voluntary movement in the rat. Electroencephalogr. Clin. Neurophysiol. *26*, 407–418.

Vanderwolf, C.H. (1988). Cerebral activity and behavior: control by central cholinergic and serotonergic systems. Int. Rev. Neurobiol. *30*, 225–340.

Wallenstein, G.V., and Hasselmo, M.E. (1997). GABAergic modulation of hippocampal population activity: sequence learning, place field development, and the phase precession effect. J. Neurophysiol. *78*, 393–408.

Winson, J. (1978). Loss of hippocampal theta rhythm results in spatial memory deficit in the rat. Science *201*, 160–163.